# Timing jitter of passively-mode-locked semiconductor lasers subject to optical feedback: A semi-analytic approach

Lina Jaurigue,[1] Alexander Pimenov,[3] Dmitrii Rachinskii,[4] Eckehard Schöll,[1] Kathy Lüdge,[1,2] and Andrei G. Vladimirov[3,5]

[1]*Institut für Theoretische Physik, Sekretariat EW 7-1, Technische Universität Berlin, Hardenbergstrasse 36, 10623 Berlin, Germany*

[2]*Department of Physics, Freie Universität Berlin, Arnimallee 14, 14195 Berlin, Germany*

[3]*Weierstrass Institute, Mohrenstrasse 39, 10117 Berlin, Germany*

[4]*Department of Mathematical Sciences, The University of Texas at Dallas, 800 West Campbell Road, Richardson, Texas 75080, USA*

[5]*Lobachevsky University of Nizhny Novgorod, 603950, Russia*

(Received 9 July 2015; published 3 November 2015)

We study the effect of delayed coherent optical feedback on the pulse timing jitter in passively-mode-locked semiconductor lasers with the help of a semi-analytical method which we develop to calculate the timing fluctuations in these lasers. Through the proposed method physical insights into the feedback dependence of the timing jitter are gained and the greatly reduced computation times allow for the investigation of the dependence of timing fluctuations over greater parameter domains. We show that resonant feedback leads to a reduction in the timing jitter and that a frequency-pulling region forms about the main resonances, within which a timing jitter reduction is observed. The width of these frequency-pulling regions increases linearly with short feedback delay times. We derive an analytic expression for the timing jitter, which predicts a monotonic decrease in the timing jitter for resonant feedback of increasing delay lengths, when timing jitter effects are fully separated from amplitude jitter effects. For long feedback cavities the decrease in timing jitter scales approximately as $1/\tau$ with increasing feedback delay time $\tau$. This behavior is not related to the stability of the system but is instead due to the influence of the noise, on the timing jitter, being reduced since the solution space is larger for increasing $\tau$.

DOI: 10.1103/PhysRevA.92.053807 PACS number(s): 42.60.Fc, 05.45.−a, 42.60.Mi, 42.55.Px

## I. INTRODUCTION

Many current and future applications require ultrahigh repetition frequency light pulse sources [1]. Among these applications most also require highly regular pulse arrival times. Mode-locked (ML) solid state lasers can fulfill these requirements. However, such devices are too expensive for large scale use. Due to this limitation extensive research has gone into semiconductor ML lasers. The most attractive mode-locking technique, due to its simplicity of production and handling, is passive mode-locking, which does not require any external rf modulation source. However, due to the absence of an external reference clock passively-ML lasers exhibit relatively large fluctuations in the temporal positions of pulses compared with a perfectly periodic pulse train [2]. This phenomenon is referred to as pulse timing jitter. Recently, it was proposed to use optical feedback to significantly reduce the timing jitter of passively-ML lasers [3–6]. Other methods of pulse stream stabilization which have been investigated include hybrid mode locking [7,8] and optical injection [9,10]. To characterize the performance of such devices, with respect to the timing regularity, the timing jitter is calculated. Experimentally this is done using the von Linde method [11], which involves integrating over the sidebands of the power spectrum of the laser output. However, for the numerical investigation of ML lasers the von Linde method can be impractical as it is computationally very expensive. In this paper we therefore propose a semi-analytical method of calculating the pulse timing jitter for a set of delay differential equations (DDEs) proposed earlier to describe passive mode-locking in semiconductor lasers [12–14]. The method is of general nature and can be used to estimate the variance of timing fluctuations in a wide range of time periodic dynamical systems described by autonomous systems of DDEs subject to weak additive noise.

Theoretical analysis of the influence of noise on ML pulses propagating in a laser cavity was first performed by Haus using a master equation [15]. In this and other works the spectral properties attributed to timing jitter were extensively studied, in particular the differences arising from stationary and nonstationary noise sources (active versus passive ML) [15–17]. Later the master equation technique of Haus was extended by taking into account the finite carrier density relaxation rate in semiconductor lasers [18]. The master equation has secant-shaped ML pulses as a solution, and a small perturbation of this state can be studied using the linearized equation of motion. The perturbed pulse is described by four parameters: the perturbations of the pulse amplitude, phase, frequency, and timing. Using the orthogonality of the solutions of the linearized equation to the solutions of the adjoint homogeneous linear system, coupled first-order differential equations of motion, driven by noise, can be written out. However, due to multiple simplifying assumptions underlying the Haus master equation, this approach is not directly applicable to the analysis of semiconductor laser devices, nor can it be used to describe coupled cavities. This is why the theoretical estimation of timing jitter in ML semiconductor lasers has been previously performed using the direct numerical simulations of traveling wave [19,20] and delay-differential equation (DDE) [5,6,21,22] models. As purely computational approaches are time consuming, the influence of noise on the dynamics of ML pulses has been studied only in limited parameter regions. In a recent paper [23] a semi-analytical method to estimate timing jitter in the DDE model [12–14] of a passively-ML semiconductor laser was proposed. This method was used to study the effect of

 

nonlinear phenomena such as bifurcations and bistability on timing jitter, and the numerical results were found to be in good qualitative agreement with experimental data. In this paper we consider a generalization of the semi-analytical method to study passively-ML lasers with multiple delayed feedback. We then use this semi-analytical method to derive a formula for the timing jitter for resonant feedback delay lengths.

In Sec. II we introduce an autonomous DDE model of a laser operating in a passive ML regime and describe the parameters used in our calculations. In Sec. III, by linearizing the model equations near the ML periodic solution and projecting the perturbation term on the neutral eigenfunctions corresponding to the time and phase shift symmetries of the unperturbed equations, we derive a semi-analytical expression for the variance of the pulse timing fluctuations [24,25]. Section IV is devoted to the comparison of the results obtained using this expression with those of direct numerical calculations of pulse timing jitter, and a derivation of the dependence of the timing jitter on the feedback delay time in the particular case of resonant feedback. Finally, in Sec. V we conclude with a brief discussion of our results.

## II. DDE MODEL

We use a DDE model for a passively-ML ring cavity laser subject to optical feedback from $M$ external cavities, based on the model introduced in [5]; a schematic diagram of the model is shown in Fig. 1 for the case of two feedback cavities. This model is an extension of the DDE model proposed in [12,14]. A detailed description and derivation of the feedback terms for a laser with a single feedback cavity can be found in [5]. The final set of three coupled delay differential equations is

$$\begin{aligned}\dot{\mathcal{E}}(t) = &-(\gamma + i\omega)\mathcal{E}(t) + \gamma R(t-T)e^{-i(\Delta\Omega+\omega)T}\mathcal{E}(t-T)\\ &+\gamma\sum_{m=1}^{M}\sum_{l=1}^{\infty}K_{m,l}e^{-ilC_m}R(t-T-l\tau_m)\\ &\times e^{-i(\Delta\Omega+\omega)(T+l\tau_m)}\mathcal{E}(t-T-l\tau_m)+D\xi(t), \qquad (1)\end{aligned}$$

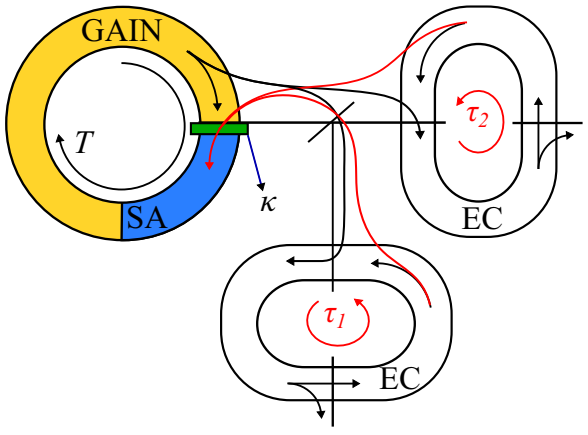


FIG. 1. (Color online) Schematic diagram of a two section ring cavity laser subject to optical feedback from two external cavities (ECs). The yellow region represents the gain section, the blue region corresponds to the saturable absorber (SA) section, and the green bar indicates the spectral filtering element.

$$\dot{G}(t) = J_g - \gamma_g G(t) - e^{-Q(t)}(e^{G(t)}-1)|\mathcal{E}(t)|^2, \qquad (2)$$

$$\dot{Q}(t) = J_q - \gamma_q Q(t) - r_s e^{-Q(t)}(e^{Q(t)}-1)|\mathcal{E}(t)|^2, \qquad (3)$$

with

$$R(t) \equiv \sqrt{\kappa}e^{(1/2)[(1-i\alpha_g)G(t)-(1-i\alpha_q)Q(t)]}. \qquad (4)$$

The dynamical variables are the slowly varying electric-field amplitude $\mathcal{E}$, the saturable gain $G$, and the saturable loss $Q$. The saturable gain $G$ and saturable loss $Q$ are related to the carrier inversion in the gain and absorber sections, respectively. In Eq. (2) $J_g$ is related to the current pumped into the gain section and $J_q$ in Eq. (3) describes the unsaturated absorption. The carrier lifetimes in the gain and absorber sections are given by $1/\gamma_g$ and $1/\gamma_q$, respectively. The factor $r_s$ is the ratio of the saturation intensities in the gain and absorber sections. The $M+1$ delay times in this system are the cold cavity round-trip time $T$ and the external cavity round-trip times (delay times) $\tau_m$ of the $M$ feedback cavities. The cold cavity round-trip time is defined as $T \equiv v/L$, where $L$ is the length of the ring cavity. The bandwidth of the laser is limited by the finite width of the gain spectrum, which is taken into account by a Lorentzian-shaped filter function of width $\gamma$. $\omega$ describes the shift between the reference frequency and the central frequency of the spectral filter. The possibility of detuning between this latter frequency and the frequency of the nearest cavity mode is allowed for by the inclusion of $\Delta\Omega$. The optical feedback is described by the sum in Eq. (1). Here $l$ is the number of round trips in the external cavity, $K_{m,l}$ is the round-trip dependent feedback strength of the $m$th feedback cavity, and $C_m$ is the phase shift that accumulates over one round trip in the external cavity. Below we consider feedback contributions only from light that has made one round trip in the external cavities ($K_{m,1} = K_m$). The last term in Eq. (1) models spontaneous emission noise using a complex Gaussian white noise term $\xi(t) = \xi_1(t) + i\xi_2(t)$ with strength $D$,

$$\langle\xi_i(t)\rangle = 0 \quad \text{and} \quad \langle\xi_i(t)\xi_j(t')\rangle = \delta_{i,j}\delta(t-t').$$

Equation (4) describes the amplification and losses of the electric field during one round trip in the laser cavity. Internal and out-coupling losses are taken into account in the attenuation factor $\kappa$ and the linewidth enhancement factors ($\alpha$ factor) in the gain and absorber sections are denoted $\alpha_g$ and $\alpha_q$, respectively.

## III. PERTURBATION ANALYSIS

Various methods of calculating the timing jitter are discussed in [6,11,20,23,26]. In this section, we consider an extension of the semi-analytical method of timing jitter estimation proposed in [23], for the DDE model of passively-ML laser, to the system (1)–(3) with external feedback and, hence, multiple delay times. The advantage of the proposed method, compared with the von Linde technique or the so-called long-term jitter calculation [6], is that it is based on the numerical solution of deterministic equations and therefore requires much shorter computation times. Furthermore, when the spontaneous emission noise is modeled by a Gaussian white noise term, the fluctuations of the pulse arrival times behave like a random walk [6], making the timing jitter

calculated from the semi-analytical method proportional to the rms timing jitter given by the von Linde method. This is useful for comparison with experiments. Details of the derivation of the semi-analytical expression for the estimation of pulse timing jitter are presented in the Appendix. As we do not use the specific form of Eqs. (1)–(3) in the derivation, the same approach can be applied to the analysis of the effect of small additive noise on stable periodic solutions in other physical systems described by autonomous DDEs with multiple delays.

We consider a periodic ML solution, $\psi_0 = (\mathrm{Re}\,\mathcal{E}_0, \mathrm{Im}\,\mathcal{E}_0, G_0, Q_0)^{\mathrm{T}}$ of the system (1)–(3) for $D = 0$, with period $T_0$. One should note that due to the rotational symmetry, there is a family of such solutions $\Gamma_\varphi\psi_0 = [\mathrm{Re}(e^{i\varphi}\mathcal{E}_0), \mathrm{Im}(e^{i\varphi}\mathcal{E}_0), G_0, Q_0]^{\mathrm{T}}$, where $\Gamma_\varphi$ denotes the corresponding matrix of rotation of the $\mathcal{E}_0$ plane. The noise perturbation is assumed to be reasonably small, $D \ll 1$, and we restrict our analysis to the situation when solutions remain at a distance of order $D$ from the torus of stable periodic solutions $\Gamma_\varphi\psi_0(t+\theta)$ at all times (that is, the probability of a large fluctuation of the solution is assumed to be negligible during the typical time interval of system observation). Under this assumption, the noise results in a slow diffusion of the time shift $\theta$ of the solution, as well as a slow diffusion of the angular variable $\varphi$. Furthermore, one expects that the variance of the time shift $\theta$ and of the variable $\varphi$ increases linearly with time, that is $\langle\theta - \bar{\theta}\rangle^2 \propto t$, which expresses a simple diffusion process [27]. We use the coefficient of proportionality in this relationship as a measure of the timing jitter. Details are explained in the Appendix.

The time shift $\theta$ of a solution can be defined in several ways [28], which, in practice, lead to equivalent or close results when applied for the evaluation of the time-shift diffusion rate. In particular, the definition of the asymptotic time shift is based on the fact that every solution $\psi(t)$ of the unperturbed system (1)–(3) with $D = 0$ converges to a periodic solution $\Gamma_\varphi\psi_0(t+\theta)$ in the limit $t \to \infty$ where the constant $\theta$, called the asymptotic time shift, and the angle $\varphi$ are specific to the initial state of the solution $\psi(t)$. Recall that states of system (1)–(3) are functions defined on the interval $[-\tau'_M, 0]$ ($\tau'_0 = T$, $\tau'_m = T + \tau_m$ for $m \geqslant 1$). The asymptotic time shift $\theta$ and the angle $\varphi$ remain constant along the trajectories of the unperturbed system. However, in the perturbed system, the asymptotic time shift $\theta$ and the angular variable $\varphi$ evolve as functions of the evolving state $\psi(t+r)$ ($r \in [-\tau'_M, 0]$).

As the dynamics are restricted to a small neighborhood of the limit cycle $\psi_0$ (and its rotations $\Gamma_\varphi\psi_0$), the evolution of the time shift can be deduced from the linearization (A1) of system Eqs. (1)–(3) around this cycle. Details on the analysis of solutions of the linear system (A1) and the resulting evolution of the time shift can be found in the Appendix. Noise results in a slow diffusion of the variables $\theta$ and $\varphi$ along the neutral periodic eigenmodes of the linearized unperturbed system (A4) with the variance proportional to time. There are two such neutral modes,

$$\begin{aligned}\delta\psi_1(t) &= [\mathrm{Re}\,\dot{\mathcal{E}}_0(t), \mathrm{Im}\,\dot{\mathcal{E}}_0(t), \dot{G}_0(t), \dot{Q}_0(t)]^{\mathrm{T}},\\ \delta\psi_2(t) &= [-\mathrm{Im}\,\mathcal{E}_0(t), \mathrm{Re}\,\mathcal{E}_0(t), 0, 0]^{\mathrm{T}},\end{aligned} \tag{5}$$

which correspond to the time shift and rotational symmetries of the unperturbed ($D = 0$) nonlinear system (1)–(3), respectively; all the other Floquet modes are exponentially decaying. Two properly normalized [see (A10)] neutral modes $\delta\psi_1^\dagger(t)$ and $\delta\psi_2^\dagger(t)$ of the adjoint linear system [see (A5)] can be used for calculating the projections of noise onto the eigendirections $\delta\psi_1$ and $\delta\psi_2$. Using the perturbation expansion with respect to the small parameter $D$, and adapting the asymptotic analysis from [10], we obtain the following equations for the noise-driven slow evolution of the time shift $\theta$ and the angular variable $\varphi$ of solutions to Eqs. (1)–(3):

$$\dot{\theta} = D\,\delta\psi_1^\dagger(t+\theta)\Gamma_{-\varphi}w(t), \quad \dot{\varphi} = D\,\delta\psi_2^\dagger(t+\theta)\Gamma_{-\varphi}w(t) \tag{6}$$

with the Langevin term $\Gamma_{-\varphi}w(t) = [\xi_1(t)\cos\varphi + \xi_2(t)\sin\varphi, -\xi_1(t)\sin\varphi + \xi_2(t)\cos\varphi, 0, 0]^{\mathrm{T}}$ and the $T_0$-periodic coefficients $\delta\psi_1^\dagger$ and $\delta\psi_2^\dagger$.

The coefficients of the Fokker-Planck equation for the joint probability density $p(t,\theta,\varphi)$ of the stochastic process (6) are also periodic with respect to time. Since, for $D \ll 1$, the probability density function $p(t,\theta,\varphi)$ changes slowly, Eq. (6) and the corresponding Fokker-Planck equation can be averaged over the period $T_0$ of the functions $\delta\psi_i^\dagger(t+\theta)$, resulting in the diffusion equation with constant coefficients [29]. The diffusion coefficient

$$\bar{d}_{11} = \frac{D^2}{T_0}\int_0^{T_0} (\delta\psi_{1,1}^\dagger(s))^2 + (\delta\psi_{1,2}^\dagger(s))^2\,ds \tag{7}$$

of the time averaged Fokker-Planck equation approximates the rate of diffusion of the time shift $\theta$ (see the Appendix). Finally, since the pulse timing jitter is usually calculated over a long time interval $n\tilde{T}_0$ with $n \gg 1$ and the average period $\tilde{T}_0 \approx T_0$, and is normalized by the number of round trips $n$, we make the estimate of timing jitter as the product of the diffusion rate by the period,

$$\sigma_{\mathrm{var}}^2 = \bar{d}_{11}T_0 = D^2\int_0^{T_0} (\delta\psi_{1,1}^\dagger(s))^2 + (\delta\psi_{1,2}^\dagger(s))^2\,ds. \tag{8}$$

This value is approximately equal to the variance of $\theta(n\tilde{T}_0)$ divided by $n \gg 1$. We note that for the number of round trips $n \geqslant 1$ that is not sufficiently large, the numerically calculated timing jitter is not approximated by (8) since the numerically calculated value is affected by amplitude noise, or, in other words, stable eigendirections play a role as well [see Fig. 2(a)].

For the case of resonant optical feedback, expression (8) for the timing jitter can be further simplified, to ascertain the dependence on the feedback delay length. This will be shown in the next section where we compare the analytic result with a numerical estimate of the timing jitter.

In this work we have only included noise contributions to the electric field to model spontaneous emission, however this semi-analytic approach can also be used to describe other noise sources. Terms corresponding to other sources of noise, such as current noise, could be added to any of the equations in the system (1)–(3), and the resulting equations of motions will have a similar form to (6). However, if the noise source is colored the formula for the diffusion coefficient, as well as the timing jitter, will be different.

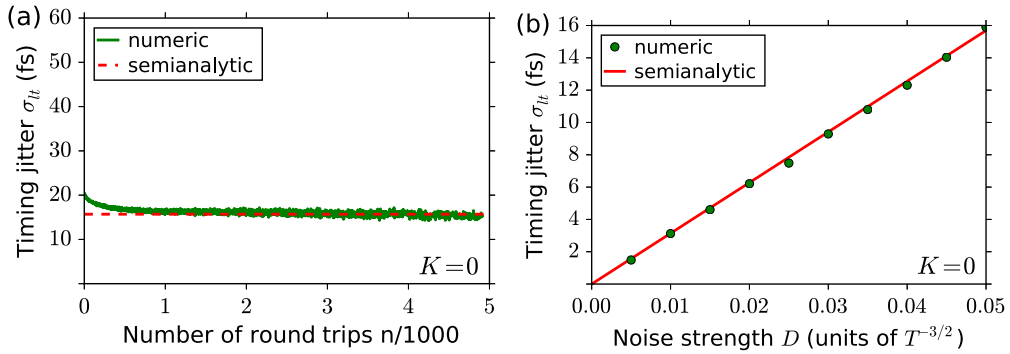


FIG. 2. (Color online) (a) Comparison of the results of numerical calculation of pulse timing jitter (green solid line), obtained for different numbers of round trips $n$, with the timing jitter value from formula (8) (red dashed line). (b) Estimation of timing jitter, calculated using formula (8) (red solid line) and the numerical method (green dots), vs noise strength $D$ in units of $T^{-3/2}$. Parameters: $K = 0$, $\tau = 0$, $T = 25$ ps, $\kappa = 0.3$, $\gamma^{-1} = 125$ fs, $\gamma_g^{-1} = 500$ ps, $\gamma_q^{-1} = 5$ ps, $s = 10$, $q_0^{-1} = 10$ ps, $g_0^{-1} = 250$ ps, $\alpha_g = 2$, $\alpha_q = 1$.

## IV. RESULTS

### A. Comparison of semi-analytical and numerical methods of timing jitter calculation.

In this section we compare the timing jitter calculated using Eq. (8) with that obtained from the variance of the pulse timing fluctuations (long-term timing jitter) through numerical integration of the stochastic system [Eqs. (1)–(3) with $D \neq 0$]. The latter (numerical) method is described in detail in [6]. We will focus mainly on the case of one feedback cavity, $M = 1$, and compare the two approaches to the timing jitter calculation at different feedback delay times ($\tau_1 \equiv \tau$) and the feedback strengths ($K_1 \equiv K$).

First, we apply the semi-analytical method of the timing jitter calculation to the case of a passively-ML semiconductor laser without feedback, i.e., $K_m \equiv 0$ in Eqs. (1)–(3). In [6] it was shown that after a sufficiently large number of round trips $n$ within the laser cavity the variance of the pulse timing fluctuations grows linearly with the round-trip number. In the numerical method the timing fluctuations are therefore calculated over many thousands of cavity round trips. In Fig. 2(a) the timing jitter is plotted as a function of the round-trip number $n$. The initial decrease of the numerically calculated timing fluctuation variance (green line) with $n$ (for small $n$) can be attributed to the impact of the eigenfunctions with $\mathrm{Re}\,\lambda < 0$ (see the Appendix). Using DDE-BIFTOOL [30], for $\gamma T \gg 1$ (or $\gamma \tau_m \gg 1$), one can typically observe that many characteristic exponents $\lambda$ of the ML solution have real parts close to 0, and, therefore, the equation of motion (A9) suggests that such exponents will have a non-negligible impact on the numerically calculated timing jitter even after many cavity round trips. Since the eigenfunctions with $\mathrm{Re}\,\lambda < 0$ are neglected in the semi-analytical approach, the value of the timing jitter estimated using this approach does not depend on $n$ [dashed red line in Fig. 2(a)]. In the limit of large $n$ this value is in agreement with the data obtained by direct numerical integration of Eqs. (1)–(3), as shown in Fig. 2(a). Figure 2(b) shows the timing jitter, obtained using both methods, in dependence of the noise strength $D$. It is seen that good quantitative agreement is obtained for small to moderate levels of noise.

Next, let us consider a system with feedback from one external cavity. Figure 3(a) shows a comparison of the timing jitter calculated from the two methods in dependence of the noise strength. For the numerical timing jitter calculation method (green dots) the timing fluctuations that arise over 40 000 round trips in the laser cavity are calculated, and the variance of these timing fluctuations is then calculated for 300 noise realizations. For the semi-analytical method (red line) the solutions to the adjoint linearized homogeneous system (A5) are numerically calculated. In both cases we simulate for a sufficiently long time (approximately 5000 round trips) before starting the calculation of the timing jitter to avoid transient effects. We find very good agreement between the results obtained using the two methods. For the simulations presented in Fig. 3(a) the feedback delay time was chosen to be resonant with the ML pulse repetition period (interspike interval time) $T_{ISI,0}$ of a solitary laser (ML laser without feedback), meaning that the condition $\tau = qT_{ISI,0}$ is fulfilled, where $q$ is an integer. Resonant feedback applied in the fundamental ML regime does not significantly affect the dynamical behavior of the system, hence the laser output remains periodic and the semi-analytic method is applicable. When the feedback delay time is tuned from one resonance to the next, bifurcations can occur and the dynamical behavior can change. This is described in detail in [31] and [5]. In Fig. 3(b) the numerically calculated dependence of the timing jitter on the delay time $\tau$ is compared to that estimated semi-analytically, spanning from the 67th to the 68th resonance ($q = 67$ and $q = 68$, respectively). Within the frequency-pulling regions of the main resonances there is very good agreement between the results obtained using the two methods. The frequency pulling regions are the $\tau$ ranges about the main resonances within which there

TABLE I. Parameter values used in numerical simulations, unless stated otherwise.

| Symbol | Value | Symbol | Value |
|---|---|---|---|
| $T$ | 25 ps | $\gamma$ | 2.66 ps$^{-1}$ |
| $\gamma_g$ | 1 ns$^{-1}$ | $\gamma_q$ | 75 ns$^{-1}$ |
| $J_g$ | 0.12 ps$^{-1}$ | $J_q$ | 0.3 ps$^{-1}$ |
| $r_s$ | 25.0 | $C_m$ | 0 |
| $\kappa$ | 0.1 | $\Delta\Omega$ | 0 |

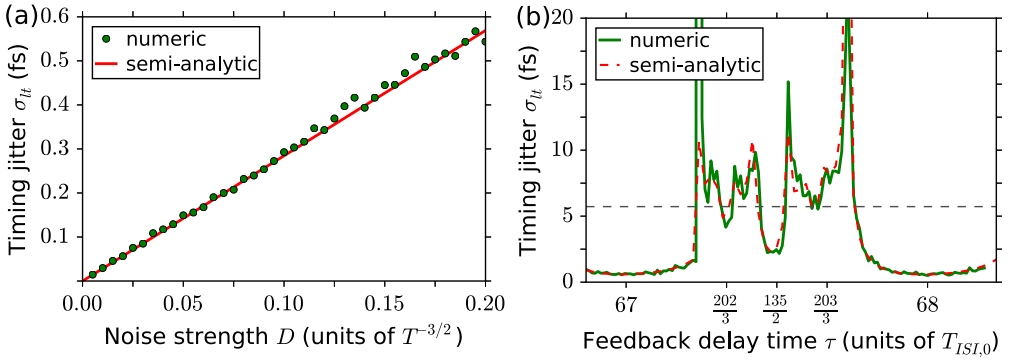


FIG. 3. (Color online) (a) Timing jitter in dependence of the noise strength, calculated using the semi-analytic method (red line) and the numerical method described in [6] (green dots) for $\tau = 70T_{ISI,0}$. (b) Timing jitter in dependence of the feedback delay time, calculated using the semi-analytic method (red dashed line) and the numerical method (green line) for $D = 0.2T^{-3/2}$. Parameters: $\alpha_g = 0$, $\alpha_q = 0$, $K = 0.1$. Other parameters are as in Table I.

is one pulse in the laser cavity and the repetition rate tunes with $\tau$ [5]. In Fig. 3(b) these regions can be identified by the low timing jitter about the main resonances. At the edges of the frequency-pulling regions there is a sharp increase in the timing jitter. This very large timing jitter coincides with saddle-node bifurcation points of the deterministic system [Eqs. (1)–(3) with $D = 0$] [6]. At the edge of the 67th resonance there is a large discrepancy between the semi-analytical and numerical methods. This is because in the stochastic system noise induced switching between bistable solutions, which arise due to the saddle-node bifurcations, occurs. Away from the bifurcation points there is good agreement between the two methods, also between the main resonances, because although the dynamical behavior changes between the main resonances, i.e., multiple feedback induced pulses, the solutions remain periodic and therefore the semi-analytical method is applicable.

For the parameters used in Fig. 3(b) the system is well behaved and the solutions are periodic, however for other parameters, particularly for larger feedback strengths and nonzero amplitude-phase coupling, this is not the case; quasiperiodic or chaotic dynamics can be observed. In such regions the semi-analytic approach is invalid, however the timing jitter calculated by numerical methods is not meaningful in these nonperiodic regions either. In Fig. 4 the timing jitter, calculated from the numerical (a) and semi-analytical (b) methods, is plotted in dependence of $K$ and $\tau$ for $\alpha_g = 2$ and $\alpha_q = 1.5$. The timing jitter is given by the color code, where blue regions indicate a reduction in the timing jitter with respect to the solitary laser, red tones indicate an increase, and white regions indicate a timing jitter greater than 20 fs, indicative of a nonperiodic pulse stream. In the black regions in Fig. 4(b) the solutions of the DDE system are nonperiodic and the semi-analytic method is not applied. Good agreement is observed between these two methods over most of the parameter range depicted. The nonperiodic regions indicated in subplot (b) coincide with the very high timing jitter estimations obtained using the numerical method.

A key difference between the two methods is that the semi-analytic method is based on the numerical simulation of deterministic equations, while the purely numerical method requires integration of a system of stochastic DDEs. Using the latter method one can run into problems that arise due

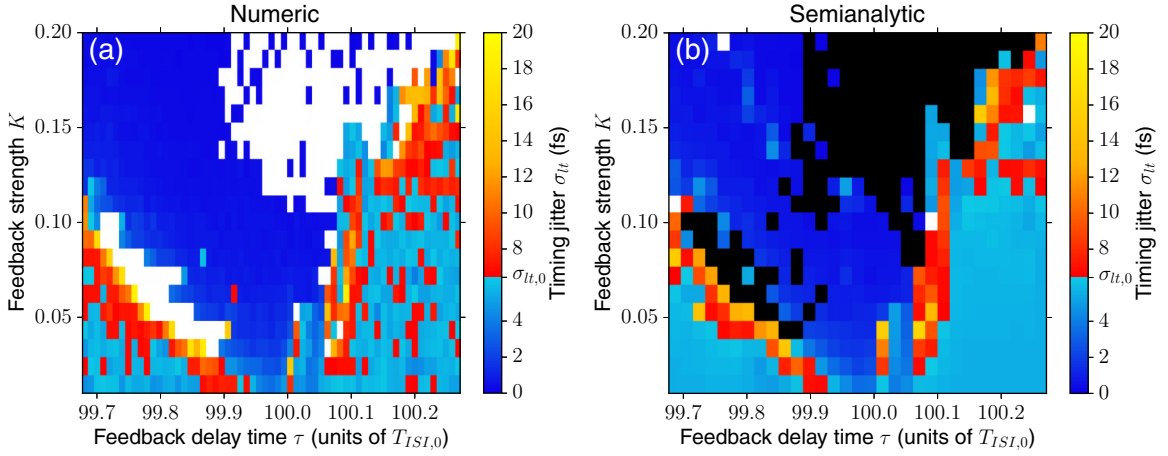


FIG. 4. (Color online) Timing jitter in dependence of the feedback cavity delay time and feedback strength, calculated numerically (a) and using the semi-analytical method (b). The timing jitter is indicated by the color code and $\sigma_{lt,0}$ is the timing jitter of the solitary laser. Regions in white indicate a timing jitter greater then 20 fs. In (b) black marks the regions where the deterministic system has a nonperiodic solution and the semi-analytical method cannot be applied. Parameters: $D = 0.2T^{-3/2}$, $\alpha_g = 2$, $\alpha_q = 1.5$; others are as in Table I.

to the multiplicity of stable solutions found in this system. Since timing jitter estimation requires averaging over many noise realizations, depending on the particular realization, due to transient effects, the system can land on different solutions. As different ML solutions can have slightly different interspike interval times, the fully numerical estimation of the timing jitter can lead to erroneously large values in such a case [22]. This makes it difficult to perform timing jitter calculations over a large parameter domain, as it is not easy to distinguish between the above-mentioned effect and a destabilization of the pulse stream due to the feedback conditions. Note that this is a different effect than switching between solutions within one time series. Such difficulties are eliminated when using the semi-analytic method, as in this case the estimation of the variance is based on the integration of deterministic equations. Therefore, there are two main advantages to using the semi-analytic method to calculate the timing jitter, compared with brute force methods involving numerical integration of stochastic differential equations. First, the aforementioned difficulties can be avoided, and second, the computation times can be greatly reduced (by over a factor of 100) as averaging over many noise realizations is not needed. This means that it can become feasible to calculate the timing jitter for longer feedback delay times, which is of interest due to the improved timing jitter reduction predicted for increased delay times [31] and for better comparison with experiments, where typically very long feedback cavities are used [4,32].

### B. Delay length dependence of timing jitter

We now use the semi-analytic method to investigate how the timing jitter decreases with increased resonant feedback delay times and how the width of the frequency-pulling regions is affected by this increase. In Fig. 5 the timing jitter is plotted as a function of $\tau$ in (a) and (b) for a short and a long $\tau$ range, respectively. The black dashed line indicates the timing jitter of the solitary laser. The delay times are plotted in units of $T_{ISI,\tau=0}$, the interspike interval time for zero delay feedback (instantaneous feedback, $\tau = 0$ and $K \neq 0$), meaning that the resonant feedback occurs at the integer delay values. ($T_{ISI,\tau=0}$ and $T_{ISI,0}$ only differ slightly. Here we choose $T_{ISI,\tau=0}$ as our reference because the period is the same for all $\tau = qT_{ISI,\tau=0}$, where $q$ is an integer, and we will use this property in subsequent calculations.) In both (a) and (b) a timing jitter reduction is observed for resonant feedback. For the longer delay times depicted in (b) the timing jitter reduction is greater and the frequency-pulling region about the main resonances is wider. Changes in the frequency-pulling regions are not discernible over small $\tau$ ranges. To show the change in dependence of $\tau$ more clearly a map of the timing jitter is shown in a $\tau$-$\tau$ plot in (c). In this plot both axes are related to the delay time, the $\tau_1$ axis shows changes over one $T_{ISI,\tau=0}$ interval, whereas the $\tau_0$ axis shows changes from one resonance to the next. For each point on this map the feedback delay time is given by $\tau = \tau_0 + \tau_1$. The $\tau_1$ axis is centered on the exact main resonances $\tau = qT_{ISI,\tau=0}$ and the $\tau_0$ axis gives the number $q$ of the main resonances. The timing jitter is given by the color code. Regions in blue and green indicate a reduction in the timing jitter with respect to the solitary laser ($K = 0$) and regions in red indicate an increase in the timing jitter. In the green regions the timing jitter is reduced by a factor of 10 or greater. For all $q$ values a reduction in the timing jitter is achieved at the exact main resonances and for increasing $q$ the decrease in the timing jitter can clearly be seen. It is seen from Fig. 5(c) that for short delays the width of the frequency-pulling regions, with reduced timing jitter, increases approximately linearly with the number $q$. The edges of the frequency pulling region are marked by the dashed black lines. At about $q = 50$ the frequency-pulling region is intersected by the solutions that correspond to higher-order resonances ($p\tau = qT_{ISI,\tau=0}$, where $p = 2,3,4,\ldots$). This is due to a bistability between the main and higher-order resonant solutions [5]. For the results presented in Fig. 5(c), the same initial conditions were used in the numerical simulations for all delay values. By performing a sweep in $\tau$ (using the previous $\tau$ solution as the initial conditions for the next $\tau$) one can stay on the main resonant solution in the bistable regions.

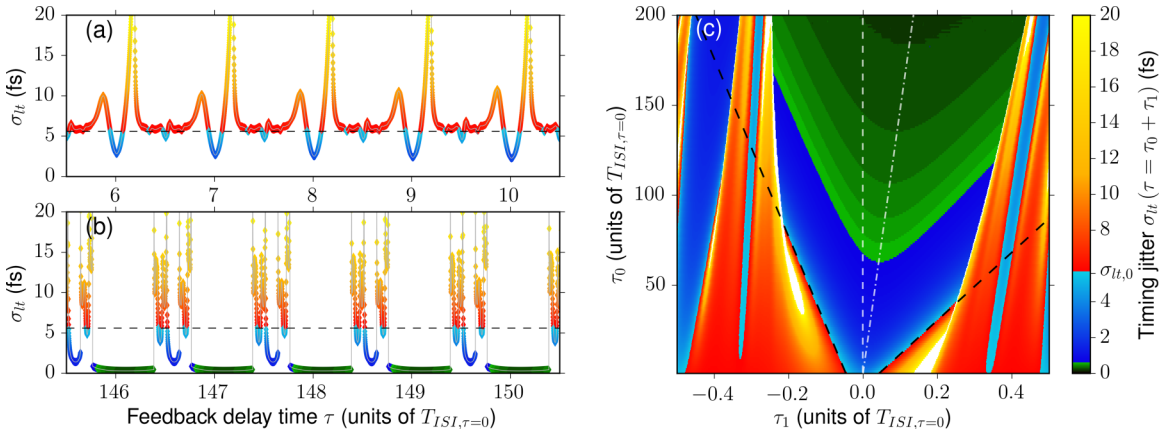


FIG. 5. (Color online) (a),(b) Timing jitter $\sigma_{lt}$ in dependence of the feedback cavity delay time. The color code indicates the timing jitter according to the color bar given in (c). The black dashed line indicates the timing jitter of the solitary laser. (c) Timing jitter $\sigma_{lt}$ in dependence of the feedback cavity delay time, where $\tau = \tau_0 + \tau_1$ for any given point. The horizontal axis spans one $T_{ISI,\tau=0}$ and is centered on an exact main resonance. The vertical axis indicates the number of the main resonance. The timing jitter is indicated by the color code and $\sigma_{lt,0}$ is the timing jitter of the solitary laser. Parameters: $K = 0.1$, $D = 0.2T^{-3/2}$, $\alpha_g = 0$, $\alpha_q = 0$; others as in Table I.

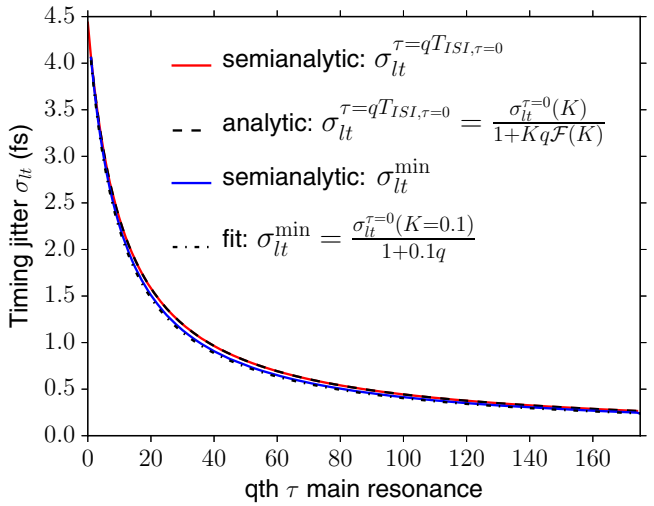


FIG. 6. (Color online) Timing jitter $\sigma_{lt}$ at the exact main resonances (red solid line) and the minimum timing jitter in each resonance region (blue solid line) as a function of the number $q$ of the main resonance, calculated using the semi-analytic method. The dashed line shows the timing jitter at the exact main resonances given by the analytic expression Eq. (13). The dot-dashed line shows the fit of Eq. (14) to the minimum timing jitter in each resonance regions. Parameters: $K = 0.1$, $D = 0.2T^{-3/2}$, $\alpha_g = 0$, $\alpha_q = 0$; others as in Table I.

In order to quantify the decrease in the timing jitter with increasing number $q$, we have plotted the timing jitter at the main resonances in Fig. 6. The red line shows the results of the semi-analytic method for the exact main resonances $\tau = qT_{ISI,\tau=0}$ [$\tau$ values corresponding to the white dashed line in Fig. 5(c)] and the blue line shows the results of the semi-analytic method for the minimum timing jitter in each main resonance frequency-pulling region [$\tau$ values corresponding to the white dot-dashed line in Fig. 5(c)]. The expression for the timing jitter at the main resonances, $\tau = qT_{ISI,\tau=0}$, can be derived analytically using Eq. (8) and the bilinear form (A6). At the exact main resonances the solutions to Eqs. (1)–(3) are identical for all $q$, and the periodicity is the same as that of the laser with zero delay (instantaneous) feedback $T_0$ ($T_{ISI,\tau=0}$). Therefore, for $\tau = qT_{ISI,\tau=0}$, Eq. (A6) can be expressed as

$$\begin{aligned}[\delta\psi^\dagger,\delta\psi](t) &= \delta\psi^\dagger(t)\delta\psi(t)\\ &+ \int_{-T}^{0} \delta\psi^\dagger(t+r+T)B_0(t+r)\delta\psi(t+r)dr\\ &+ K\int_{-T}^{0} \delta\psi^\dagger(t+r+T)B_1(t+r)\delta\psi(t+r)dr\\ &+ K\int_{-T-qT_{ISI,\tau=0}}^{-T} \delta\psi^\dagger(t+r+T)B_1(t+r)\delta\psi(t+r)dr. \quad (9)\end{aligned}$$

The last term on the right-hand side can be further simplified due to the time shift invariance and periodicity of the integrand, giving

$$[\delta\psi^\dagger,\delta\psi] = [\delta\psi^\dagger,\delta\psi]^{\tau=0} + Kq\int_{-T_{ISI,\tau=0}}^{0} [\delta\psi^\dagger(t+r+T)]^{\mathrm{T}} B_1(t+r)\delta\psi(t+r)dr, \quad (10)$$

where the first three terms on the right-hand side of Eq. (9) are now expressed as $[\delta\psi^\dagger,\delta\psi]^{\tau=0}$, which is the bilinear form for $\tau = 0$ ($q = 0$). Equation (8) can thus be expressed as

$$\sigma_{\mathrm{var}} = \sqrt{D^2\int_0^{T_0}\left(\frac{\delta\psi_{1,1}^{\dagger *}(t)}{[\delta\psi_1^{\dagger *},\delta\psi_1^{*}]^{\tau=0} + Kq\mathcal{F}'(K)}\right)^2 + \left(\frac{\delta\psi_{1,2}^{\dagger *}(t)}{[\delta\psi_1^{\dagger *},\delta\psi_1^{*}]^{\tau=0} + Kq\mathcal{F}'(K)}\right)^2 dt}, \quad (11)$$

where $\frac{\delta\psi_1^{(\dagger)*}}{[\delta\psi_1^{\dagger *},\delta\psi_1^{*}]} = \delta\psi_1^{(\dagger)}$ and

$$\mathcal{F}'(K) = \int_{-T_{ISI,\tau=0}}^{0} \delta\psi_1^{\dagger *}(t+r+T)B_1(t+r)\delta\psi_1^{*}(t+r)dr,$$

which is a function of $K$ but not of $\tau$. Finally, Eq. (11) can be simplified to

$$\sigma_{\mathrm{var}} = \frac{1}{1+Kq\mathcal{F}'(K)}\sqrt{D^2\int_0^{T_0}\left(\delta\psi_{1,1}^{\dagger\tau=0}(t)\right)^2 + \left(\delta\psi_{1,2}^{\dagger\tau=0}(t)\right)^2 dt}, \quad (12)$$

where $\delta\psi_1^{\dagger\tau=0} = (\delta\psi_{1,1}^{\dagger\tau=0},\delta\psi_{1,2}^{\dagger\tau=0},\delta\psi_{1,3}^{\dagger\tau=0},\delta\psi_{1,4}^{\dagger\tau=0})^{\mathrm{T}}$ is the solution fulfilling the biorthogonality condition for $\tau = 0$ and $\mathcal{F}(K) = \frac{\mathcal{F}'(K)}{[\delta\psi_1^{\dagger *},\delta\psi_1^{*}]^{\tau=0}}$. The timing jitter for resonant feedback, $\tau = qT_{ISI,\tau=0}$, is therefore given by

$$\sigma_{lt}^{\tau=qT_{ISI,\tau=0}} = \frac{\sigma_{lt}^{\tau=0}(K)}{1+Kq\mathcal{F}(K)}, \quad (13)$$

where $\sigma_{lt}^{\tau=0}(K)$ is the timing jitter for $\tau = 0$. The curve obtained using this analytic expression is shown by the dashed black line in Fig. 6. A formula for the minimum jitter cannot be derived in the same way as the interspike interval time changes with $q$. However, fitting the minimum jitter curve for various feedback strengths we find that the relation

$$\sigma_{lt}^{\min} \approx \frac{\sigma_{lt}^{\tau=0}(K)}{1+Kq} \quad (14)$$

holds well for low feedback strengths. The fit is plotted in the black dot-dashed line in Fig. 6.

Several physical insights can be gained from Eqs. (13) and (14). First, the decrease in the timing jitter, with increasing delay length, is directly related to the increase in the length of the history of the solution. The influence on the dynamics of the system, of a perturbation, at one time point is smaller if the solution space is larger. This can be understood by considering the definition of the asymptotic time shift. If the solution to the homogeneous system is perturbed at one point in time, then as $t \to \infty$ the solution will once again converge to the solution of the homogeneous system, but with some time shift with respect to the solution before the perturbation. If the solution space is larger then the resulting time shift will be smaller. Another way to think of this is to consider that the pulse positions are correlated over the history of the solution. If the pulse positions are correlated over longer time spans, via increased feedback delay lengths, then the timing jitter is decreased. The timing jitter reduction therefore has nothing to do with the stability of the system, as one might have expected based on studies on feedback stabilization [33]. Second, in contrast to previous works on timing jitter reduction these results highlight the importance of the pulse shape, and hence the gain and absorber dynamics. The pulse shape enters in the integral for $\mathcal{F}(K)$, as this influences the overlap of $\delta\psi_{0t}^{\dagger}(t+T)$ and $B_1(t)\delta\psi_1(t)$. This overlap is greatest when $T_{ISI} = T$, and the deviation of the period from the cold cavity round-trip time is intrinsically linked to the asymmetry of the pulses. Increasing the width of the Lorentzian filter reduces the interspike interval time, as $T_{ISI} \approx T + \gamma^{-1}$ [14], this results in an increase in $\mathcal{F}(K)$, and hence improved timing jitter reduction at the exact main resonance. The fact that the minimum timing jitter does not coincide with the exact main resonances shows that pulse reshaping also leads to a timing jitter reduction.

In the derivation of Eq. (13) contributions to the timing jitter from eigenfunctions with negative eigenvalues, $\lambda < 0$, are neglected. However, for increased feedback delay lengths, the number of weakly stable Floquet multipliers close to 1 increases. This leads to long transients in numerical simulations of the deterministic system [Eqs. (1)–(3) $D = 0$]. These transient effects are accompanied by fluctuations in the pulse heights, which have the periodicity of the feedback delay time. Including noise in the system excites these transient amplitude fluctuations, which results in an increased timing jitter, as, via the interaction with the gain and absorber media, changes in the pulse height also lead to slight changes in the pulse positions. Such noise induced effects were observed experimentally as side peaks in the phase noise spectra [32,34,35]. Equation (13) is therefore only valid in the limit in which such effects can be neglected. For the parameter values used in our simulations Eq. (13) holds for up to $q \approx 300$. However, Eq. (13) still gives a lower limit for the timing jitter reduction that is achieved, if the noise induced fluctuations can be suppressed. Similarly, we note that our approach might not produce quantitatively accurate results near the points of bifurcations, where weakly damped modes are also present in the system, and, hence additional degrees of freedom must be taken into account. The extension of the method to the describe this situation will be the subject of the future work.

## V. CONCLUSIONS

We have investigated the influence of optical feedback on the timing jitter of a passively-ML semiconductor laser. For resonant feedback we have derived an expression, Eq. (13), for the analytical dependence of the timing jitter on the feedback delay length, showing that the timing jitter drops off as approximately $1/\tau$ for $\tau \gg T$, as long as amplitude jitter effects can be neglected. This trend is directly related to the increase in the history of the solutions, which results in the influence of the noise being reduced and the pulse positions being correlated over longer times. Around the main resonant feedback delay lengths, frequency-pulling regions form, in which the timing jitter is reduced with respect to the solitary laser. The minimum timing jitter in these regions is achieved by pulse reshaping, in addition to the correlation effects. For small feedback strengths $K$ the widths of these frequency-pulling regions increase linearly with the number $q$ of the main resonance.

These results were obtained using a semi-analytical method, presented in this paper, of calculating timing fluctuations in a DDE system describing the dynamics of a passively-ML semiconductor laser subject to optical feedback from an arbitrary number of feedback cavities. The semi-analytical method shows good agreement with methods based on direct numerical integration of the stochastic model. This method has the advantage of greatly reduced computation times and allows for achieving greater physical insights than from direct numerical computations.

## ACKNOWLEDGMENTS

The authors are thankful to D. Turaev for a very useful discussion of the asymptotic analysis method. L.J. thanks B. Lingnau for fruitful discussions and acknowledges support from the GRK 1558 funded by the DFG. A.P. and A.G.V. acknowledge the support of SFB 787 of the DFG, project B5. A.G.V. also acknowledges the support of 14-41-00044 of RSF at the Lobachevsky University of Nizhny Novgorod. D.R. acknowledges the support of NSF through Grant No. DMS-1413223.

## APPENDIX: DERIVATION OF THE EXPRESSION FOR THE RATE OF THE TIME-SHIFT DIFFUSION

Here we derive formula (7) for the time-shift diffusion rate. Recall that $\psi_0(t)$ is a $T_0$-periodic ML solution of system (1)–(3). Substituting the expression $\psi(t) = \psi_0(t) + \delta\psi(t)$ into this system, we obtain the linearized equations

$$\frac{d}{dt}\delta\psi(t) = A(t)\delta\psi(t) + \sum_{m=0}^{M} B_m(t-\tau_m')\delta\psi(t-\tau_m') + Dw(t), \tag{A1}$$

where $A$ and $B_m$ are $T_0$-periodic Jacobi matrices of the linearization; $\tau_0' = T$, $\tau_m' = T + \tau_m$ for $m \geqslant 1$; and, $Dw(t) = D[\xi_1(t),\xi_2(t),0,0]^{\mathrm{T}}$ is the small noise term. The matrices $A(t)$

and $B_m(\theta)$ are

$$A(t) = \begin{pmatrix} -\gamma & -\omega & 0 & 0 \\ \omega & -\gamma & 0 & 0 \\ e^{-Q_0(t)}\mathcal{G}(t)2\mathcal{E}_0^R(t) & e^{-Q_0(t)}\mathcal{G}(t)2\mathcal{E}_0^I(t) & -\gamma_g - e^{-Q_0(t)}e^{G_0(t)}|\mathcal{E}_0(t)|^2 & -e^{-Q_0(t)}\mathcal{G}(t)|\mathcal{E}_0(t)|^2 \\ -r_s\mathcal{Q}(t)2\mathcal{E}_0^R(t) & -r_s\mathcal{Q}(t)2\mathcal{E}_0^I(t) & 0 & -\gamma_q - r_s e^{-Q_0(t)}|\mathcal{E}_0(t)|^2 \end{pmatrix} \tag{A2}$$

with $\mathcal{G}(t) = 1 - e^{G_0(t)}$ and $\mathcal{Q}(t) = 1 - e^{Q_0(t)}$, and

$$B_m(\theta) = K_m\gamma \begin{pmatrix} R_0^R(\theta) & -R_0^I(\theta) & R_0^R(\theta)\mathcal{E}_{RI}^g(\theta) - R_0^I(\theta)\mathcal{E}_{IR}^g(\theta) & -R_0^R(\theta)\mathcal{E}_{RI}^q(\theta) + R_0^I(\theta)\mathcal{E}_{IR}^q(\theta) \\ R_0^I(\theta) & R_0^R(\theta) & R_0^I(\theta)\mathcal{E}_{RI}^g(\theta) + R_0^R(\theta)\mathcal{E}_{IR}^g(\theta) & -R_0^I(\theta)\mathcal{E}_{RI}^q(\theta) - R_0^R(\theta)\mathcal{E}_{IR}^q(\theta) \\ 0 & 0 & 0 & 0 \\ 0 & 0 & 0 & 0 \end{pmatrix} \tag{A3}$$

for $\theta = t - \tau_m'$ and $K_0 = 1$, with $\mathcal{E}_0^R = \mathrm{Re}\,\mathcal{E}_0$, $\mathcal{E}_0^I = \mathrm{Im}\,\mathcal{E}_0$, $R_0(\theta) = \sqrt{\kappa}e^{(1/2)(1-i\alpha_g)G_0(\theta)-(1/2)(1-i\alpha_q)Q_0(\theta)-i\omega(\theta-t)}$, $R_0^R = \mathrm{Re}\,R_0$, $R_0^I = \mathrm{Im}\,R_0\mathcal{E}_{RI}^g(\theta) = \frac{1}{2}(\mathcal{E}_0^R(\theta) + \alpha_g\mathcal{E}_0^I(\theta))$, $\mathcal{E}_{IR}^g(\theta) = \frac{1}{2}(\mathcal{E}_0^I(\theta) - \alpha_g\mathcal{E}_0^R(\theta))$, $\mathcal{E}_{RI}^q(\theta) = \frac{1}{2}(\mathcal{E}_0^R(\theta) + \alpha_q\mathcal{E}_0^I(\theta))$, and $\mathcal{E}_{IR}^q(\theta) = \frac{1}{2}(\mathcal{E}_0^I(\theta) - \alpha_q\mathcal{E}_0^R(\theta))$.

When there is no noise ($D = 0$), the homogeneous system

$$-\frac{d}{dt}\delta\psi(t) + A(t)\delta\psi(t) + \sum_{m=0}^{M} B_m(t-\tau_m')\delta\psi(t-\tau_m') = 0 \tag{A4}$$

and its adjoint system, for a row vector $\delta\psi^\dagger(t) = (\delta\psi_1^\dagger, \delta\psi_2^\dagger, \delta\psi_3^\dagger, \delta\psi_4^\dagger)$,

$$\frac{d}{dt}\delta\psi^\dagger(t) + \delta\psi^\dagger(t)A(t) + \sum_{m=0}^{M}\delta\psi^\dagger(t+\tau_m')B_m(t) = 0, \tag{A5}$$

have characteristic solutions (eigenmodes) of the form $\delta\psi(t) = \delta\psi_\lambda(t) = e^{\lambda t}p_\lambda(t)$ and $\delta\psi^\dagger(t) = \delta\psi_\lambda^\dagger(t) = e^{-\lambda t}p_\lambda^\dagger(t)$, respectively, where functions $p_\lambda(t)$ and $p_\lambda^\dagger(t)$ are $T_0$ periodic and the complex value $\lambda$ is a Floquet exponent of (A4). The bilinear form [24,25]

$$[\delta\psi^\dagger,\delta\psi](t) = \delta\psi^\dagger(t)\delta\psi(t) + \sum_{m=1}^{M}\int_{-\tau_m'}^{0}\delta\psi^\dagger(t+r+\tau_m')B_m(t+r)\delta\psi(t+r)dr \tag{A6}$$

is instrumental in quantifying the effect of noise along different eigendirections $\delta\psi_\lambda(t)$ for the perturbed system (A1), because for every solution $\delta\psi(t)$ of (A1) and every solution $\delta\psi^\dagger(t)$ of (A5) the following relation holds at all times:

$$\frac{d[\delta\psi^\dagger,\delta\psi](t)}{dt} = D\delta\psi^\dagger(t)w(t). \tag{A7}$$

Indeed,

$$\begin{aligned}
\frac{d}{dt}[\delta\psi^\dagger,\delta\psi](t) &= \frac{d}{dt}\left(\delta\psi^\dagger(t)\delta\psi(t) + \sum_m\int_{-\tau_m'}^{0}\delta\psi^\dagger(s+t+\tau_m')B_m(s+t)\delta\psi(s+t)ds\right) \\
&= \frac{d\delta\psi^\dagger(t)}{dt}\delta\psi(t) + \delta\psi^\dagger(t)\frac{d\delta\psi(t)}{dt} + \frac{d}{dt}\sum_m\int_{t-\tau_m'}^{t}\delta\psi^\dagger(s+\tau_m')B_m(s)\delta\psi(s)ds \\
&= -\left(\delta\psi^\dagger(t)A(t) + \sum_m\delta\psi^\dagger(t+\tau_m')B_m(t)\right)\delta\psi(t) + \delta\psi^\dagger(t)\left(A(t)\delta\psi(t) + \sum_m B_m(t-\tau_m')\delta\psi(t-\tau_m') + w(t)\right) \\
&\quad + \sum_m[\delta\psi^\dagger(t+\tau_m')B_m(t)\delta\psi(t) - \delta\psi^\dagger(t)B_m(t-\tau_m')\delta\psi(t-\tau_m')] \\
&= D\,\delta\psi^\dagger(t)w(t).
\end{aligned}$$

In particular, for every pair of solutions of the homogeneous systems (A4) and (A5) ($D = 0$), the form $[\delta\psi^\dagger,\delta\psi](t)$ is independent of time. Equation (A7) also ensures the biorthogonality property

$$[\delta\psi_\lambda^\dagger,\delta\psi_\mu](t) \equiv 0 \tag{A8}$$

for any pair of eigenfunctions of problems (A4) and (A5) with $\lambda \neq \mu$. Furthermore, Eq. (A7) implies that for any solution $\delta\psi(t)$ of the inhomogeneous problem (A1), the projection $y_\lambda(t) = e^{\lambda t}[\delta\psi_\lambda^\dagger,\delta\psi](t)$ satisfies the equation

$$\frac{dy_\lambda(t)}{dt} = \lambda y_\lambda(t) + Dp_\lambda^\dagger(t)w(t) \tag{A9}$$

with the Langevin term $w(t)$. For $\mathrm{Re}\,\lambda < 0$, this equation defines an Ornstein-Uhlenbeck-type process with a uniformly bounded variance of order $D^2$. On the other hand, for

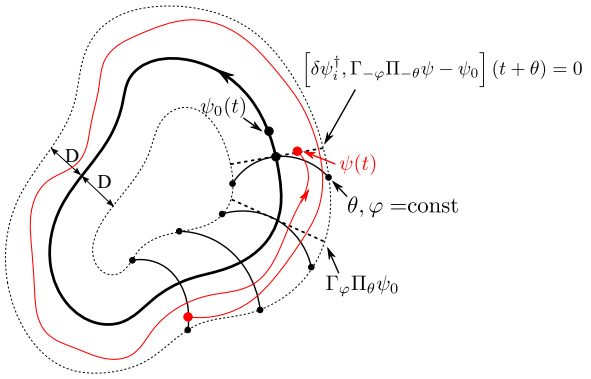


FIG. 7. (Color online) State space of the system. The bold line represent the two-dimensional toroidal surface (torus) that consists of the periodic trajectory of the ML solution $\psi_0$ and its shifts $\Gamma_\varphi\Pi_\theta\psi_0$. Trajectories of the unperturbed system starting in a neighborhood of this torus spiral towards periodic trajectories on the torus with time. Thin solid lines represent codimension 2 surfaces of constant limit time-shift and angular phase $\theta,\varphi = \text{const}$ that are transversal to the torus. Trajectories of the unperturbed system starting at any one such surface simultaneously will always return to this surface simultaneously in the future. Dashed line shows the codimension 2 surface defined by Eq. (A11), which is tangent to a surface $\theta,\varphi =$ const at the intersection point of this surface with the torus $\Gamma_\varphi\Pi_\theta\psi_0$. The red line shows a trajectory of the perturbed system.

$\lambda = 0$, we obtain a process similar to the Brownian motion with the variance that grows linearly with time as $D^2 t$. Hence, noise mostly affects the projections of a solution of (A1) onto the neutral eigenmodes (5) that have $\lambda = 0$. The two corresponding adjoint neutral eigenfunctions [that is, $T_0$-periodic solutions of the adjoint system (A5)] can be normalized in such a way as to satisfy the relations

$$[\delta\psi_1^\dagger,\delta\psi_1](t) = [\delta\psi_2^\dagger,\delta\psi_2](t) \equiv 1,$$
$$[\delta\psi_1^\dagger,\delta\psi_2](t) = [\delta\psi_2^\dagger,\delta\psi_1](t) \equiv 0. \tag{A10}$$

For stable mode-locked solutions $\psi_0(t)$ all the nonzero Floquet exponents of the linearized system have negative real parts.

Using the linearization, we can approximate the asymptotic time shift of a solution to the nonlinear system (1)–(3) by the formulas

$$[\delta\psi_1^\dagger,\Gamma_{-\varphi}\Pi_{-\theta}\psi - \psi_0](t+\theta)$$
$$= [\delta\psi_2^\dagger,\Gamma_{-\varphi}\Pi_{-\theta}\psi - \psi_0](t+\theta) = 0, \tag{A11}$$

where $\Pi_{-\theta}\psi(t) = \psi(t-\theta)$ is the time shift operator. These equations define the time shift $\theta$ and the angular phase $\varphi$ implicitly for any given state $\psi(t+r)$ ($r \in [-\tau'_M,0]$) of the nonlinear system. Geometrically, (A11) is a codimension 2 linear subspace which is tangent to the codimension 2 surface of constant asymptotic time shift $\theta$ and constant asymptotic angular phase $\varphi$ at the point where this surface intersects the torus of shifted periodic solutions $\Gamma_\varphi\Pi_\theta\psi_0$ in the state space of the system (see Fig. 7). As we consider solutions that remain within a small distance of order $D$ from this torus, the error between the asymptotic time shift and its approximation (A11) is of next order $D^2$. Also, note that Eq. (A11) themselves can be used as an alternative definition of the time shift, because these equations define a foliation of a small tubular neighborhood surrounding the torus of periodic solutions by nonintersecting surfaces $\theta = \text{const}$, $\varphi = \text{const}$.

In order to derive the equation for the evolution of the time shift, we calculate the partial derivatives of Eq. (A11) with respect to $t,\theta,\varphi$. Using symmetry, one obtains from Eqs. (A6) and (A7) the relationship

$$\frac{\partial}{\partial t}[\delta\psi_i^\dagger,\Gamma_{-\varphi}\Pi_{-\theta}\psi - \psi_0](t+\theta) = D\,\delta\psi_i^\dagger(t+\theta)\Gamma_{-\varphi}w(t) \tag{A12}$$

for $i = 1,2$. When differentiating the bilinear form $[\delta\psi_i^\dagger,\Gamma_{-\varphi}\Pi_{-\theta}\psi - \psi_0](t+\theta)$ with respect to $\theta$ and $\varphi$, we omit the terms that are proportional to $\psi - \Gamma_\varphi\Pi_\theta$, because these terms are of the order $D$ in the small vicinity of the cycle that we consider. In this approximation, we obtain

$$\frac{\partial}{\partial\theta}[\delta\psi_i^\dagger,\Gamma_{-\varphi}\Pi_{-\theta}\psi - \psi_0](t+\theta) = -[\delta\psi_i^\dagger,\delta\psi_1](t+\theta), \tag{A13}$$

$$\frac{\partial}{\partial\varphi}[\delta\psi_i^\dagger,\Gamma_{-\varphi}\Pi_{-\theta}\psi - \psi_0](t+\theta) = -[\delta\psi_i^\dagger,\delta\psi_2](t+\theta). \tag{A14}$$

Combining relationships (A10) and (A12)–(A14) with the equation

$$\left(\frac{\partial}{\partial t} + \dot\theta\frac{\partial}{\partial\theta} + \dot\varphi\frac{\partial}{\partial\varphi}\right)[\delta\psi_i^\dagger,\Gamma_{-\varphi}\Pi_{-\theta}\psi - \psi_0](t+\theta) = 0$$

[obtained by differentiating Eqs. (A11) with respect to time], we arrive at the coupled system of stochastic equations (6) that describe the slow evolution of the variables $\theta$ and $\varphi$.

Finally, using the Feynman-Kac formula, we obtain the Fokker-Planck equation for the joint probability density $p(t,\theta,\varphi)$ of the stochastic process (6):

$$\frac{\partial p}{\partial t} = \left(\frac{1}{2}\frac{\partial^2}{\partial\theta^2}(d_{11}\,p) + \frac{\partial^2}{\partial\theta\partial\varphi}(d_{12}\,p) + \frac{1}{2}\frac{\partial^2}{\partial\varphi^2}(d_{22}\,p)\right). \tag{A15}$$

This equation has variable diffusion coefficients

$$d_{11} = D^2((\delta\psi_{1,1}^\dagger)^2 + (\delta\psi_{1,2}^\dagger)^2)(t+\theta),$$
$$d_{22} = D^2((\delta\psi_{2,1}^\dagger)^2 + (\delta\psi_{2,2}^\dagger)^2)(t+\theta),$$
$$d_{12} = D^2(\delta\psi_{1,1}^\dagger\delta\psi_{2,1}^\dagger + \delta\psi_{1,2}^\dagger\delta\psi_{2,2}^\dagger)(t+\theta),$$

where $\delta\psi_{i,k}^\dagger$ are the coordinates of the four-dimensional vector functions $\delta\psi_i^\dagger$. Since, for $D \ll 1$, the probability density changes slowly, Eq. (A15) can be averaged over the period $T_0$ of the functions $d_{ij}(t+\theta)$, resulting in the diffusion equation with constant coefficients $\bar d_{ij}$ (see, for example, [29]). The averaged coefficient $\bar d_{11}$ that approximates the rate of diffusion of the time shift $\theta$ is defined by formula (7).

[1] E. U. Rafailov, M. A. Cataluna, and W. Sibbett, Mode-locked quantum-dot lasers, Nat. Photon. **1**, 395 (2007).

[2] C. Y. Lin, F. Grillot, Y. Li, R. Raghunathan, and L. F. Lester, Characterization of timing jitter in a 5 GHz quantum

dot passively mode-locked laser, Opt. Express **18**, 21932 (2010).
[3] O. Solgaard and K. Y. Lau, Optical feedback stabilization of the intensity oscillations in ultrahigh-frequency passively modelocked monolithic quantum-well lasers, IEEE Photon. Technol. Lett. **5**, 1264 (1993).
[4] C. Y. Lin, F. Grillot, N. A. Naderi, Y. Li, and L. F. Lester, rf linewidth reduction in a quantum dot passively mode-locked laser subject to external optical feedback, Appl. Phys. Lett. **96**, 051118 (2010).
[5] C. Otto, K. Lüdge, A. G. Vladimirov, M. Wolfrum, and E. Schöll, Delay induced dynamics and jitter reduction of passively mode-locked semiconductor laser subject to optical feedback, New J. Phys. **14**, 113033 (2012).
[6] C. Otto, L. C. Jaurigue, E. Schöll, and K. Lüdge, Optimization of timing jitter reduction by optical feedback for a passively mode-locked laser, IEEE Photon. J. **6**, 1501814 (2014).
[7] G. Fiol, D. Arsenijević, D. Bimberg, A. G. Vladimirov, M. Wolfrum, E. A. Viktorov, and P. Mandel, Hybrid mode-locking in a 40 GHz monolithic quantum dot laser, Appl. Phys. Lett. **96**, 011104 (2010).
[8] R. Arkhipov, A. Pimenov, M. Radziunas, D. Rachinskii, A. G. Vladimirov, D. Arsenijević, H. Schmeckebier, and D. Bimberg, Hybrid mode locking in semiconductor lasers: Simulations, analysis, and experiments, IEEE J. Quantum Electron. **19**, 1100208 (2013).
[9] N. Rebrova, T. Habruseva, G. Huyet, and S. P. Hegarty, Stabilization of a passively mode-locked laser by continuous wave optical injection, Appl. Phys. Lett. **97**, 1 (2010).
[10] N. Rebrova, G. Huyet, D. Rachinskii, and A. G. Vladimirov, Optically injected mode-locked laser, Phys. Rev. E **83**, 066202 (2011).
[11] D. von der Linde, Characterization of the noise in continuously operating mode-locked lasers, Appl. Phys. B **39**, 201 (1986).
[12] A. G. Vladimirov, D. Turaev, and G. Kozyreff, Delay differential equations for mode-locked semiconductor lasers, Opt. Lett. **29**, 1221 (2004).
[13] A. G. Vladimirov and D. Turaev, New model for mode-locking in semiconductor lasers, Radiophys. Quantum Electron. **47**, 769 (2004).
[14] A. G. Vladimirov and D. Turaev, Model for passive mode locking in semiconductor lasers, Phys. Rev. A **72**, 033808 (2005).
[15] H. A. Haus and A. Mecozzi, Noise of mode-locked lasers, IEEE J. Quantum Electron. **29**, 983 (1993).
[16] D. Eliyahu, R. A. Salvatore, and A. Yariv, Noise characterization of a pulse train generated by actively mode-locked lasers, J. Opt. Soc. Am. B **13**, 1619 (1996).
[17] D. Eliyahu, R. A. Salvatore, and A. Yariv, Effect of noise on the power spectrum of passively mode-locked lasers, J. Opt. Soc. Am. B **14**, 167 (1997).
[18] L. A. Jiang, M. E. Grein, H. A. Haus, and E. P. Ippen, Noise of mode-locked semiconductor lasers, IEEE J. Sel. Top. Quantum Electron. **7**, 159 (2001).
[19] B. Zhu, I. H. White, R. V. Penty, A. Wonfor, E. Lach, and H. D. Summers, Theoretical analysis of timing jitter in monolithic multisection mode-locked dbr laser diodes, IEEE J. Quantum Electron. **33**, 1216 (1997).
[20] J. Mulet and J. Mørk, Analysis of timing jitter in external-cavity mode-locked semiconductor lasers, IEEE J. Quantum Electron. **42**, 249 (2006).
[21] L. C. Jaurigue, E. Schöll, and K. Lüdge, Passively mode-locked laser coupled to two external feedback cavities, Proc. SPIE **9382**, 93820B (2015).
[22] C. Simos, H. Simos, C. Mesaritakis, A. Kapsalis, and D. Syvridis, Pulse and noise properties of a two section passively mode-locked quantum dot laser under long delay feedback, Opt. Commun. **313**, 248 (2014).
[23] A. S. Pimenov, T. Habruseva, D. Rachinskii, S. P. Hegarty, G. Huyet, and A. G. Vladimirov, The effect of dynamical instability on timing jitter in passively mode-locked quantum-dot lasers, Opt. Lett. **39**, 6815 (2014).
[24] A. Halanay, *Differential Equations: Stability, Oscillations, Time Lags* (Academic, New York, 1966).
[25] J. K. Hale, *Theory of Functional Differential Equations* (Springer, New York, 1977).
[26] F. Kefelian, S. O'Donoghue, M. T. Todaro, J. G. McInerney, and G. Huyet, RF linewidth in monolithic passively mode-locked semiconductor laser, IEEE Photon. Technol. Lett. **20**, 1405 (2008).
[27] A. Daffertshofer, Effects of noise on the phase dynamics of nonlinear oscillators, Phys. Rev. E **58**, 327 (1998).
[28] L. Callenbach, P. Hänggi, S. J. Linz, J. A. Freund, and L. Schimansky-Geier, Oscillatory systems driven by noise: Frequency and phase synchronization, Phys. Rev. E **65**, 051110 (2002).
[29] M. S. Krol, On the averaging method in nearly time-periodic advection-diffusion problems, SIAM J. Appl. Math. **51**, 1622 (1991).
[30] K. Engelborghs, T. Luzyanina, and G. Samaey, DDE-BIFTOOL v. 2.00: a matlab package for bifurcation analysis of delay differential equations, Technical Report TW-330, Department of Computer Science, K. U. Leuven, Belgium, 2001.
[31] C. Otto, *Dynamics of Quantum Dot Lasers – Effects of Optical Feedback and External Optical Injection*, Springer Theses (Springer, Heidelberg, 2014).
[32] D. Arsenijević, M. Kleinert, and D. Bimberg, Phase noise and jitter reduction by optical feedback on passively mode-locked quantum-dot lasers, Appl. Phys. Lett. **103**, 231101 (2013).
[33] K. Pyragas, Continuous control of chaos by self-controlling feedback, Phys. Lett. A **170**, 421 (1992).
[34] M. Haji, L. Hou, A. E. Kelly, J. Akbar, J. H. Marsh, J. M. Arnold, and C. N. Ironside, High frequency optoelectronic oscillators based on the optical feedback of semiconductor mode-locked laser diodes, Opt. Express **20**, 3268 (2012).
[35] L. Drzewietzki, S. Breuer, and W. Elsäßer, Timing jitter reduction of passively mode-locked semiconductor lasers by self- and external-injection: Numerical description and experiments, Opt. Express **21**, 16142 (2013).